Optimum UV Disinfection between Concentric Cylinders

ARTICLE *in* INDUSTRIAL & ENGINEERING CHEMISTRY RESEARCH · JANUARY 2008

Impact Factor: 2.59

3 AUTHORS, INCLUDING:

Tatiana Koutchma
Agriculture and Agri-Food Canada
88 PUBLICATIONS **954** CITATIONS
SEE PROFILE

Zhengcai Ye
Aramco Services Company
9 PUBLICATIONS **69** CITATIONS
SEE PROFILE

Article

Optimum UV Disinfection between Concentric Cylinders

Z. Ye, and L. J. ForneyT. KoutchmaA. T. Giorges, and J. A. Pierson

Ind. Eng. Chem. Res., **2008**, 47 (10), 3444-3452 • DOI: 10.1021/ie0703641

Optimum UV Disinfection between Concentric Cylinders

Z. Ye and L. J. Forney*

School of Chemical & Biomolecular Engineering, Georgia Institute of Technology, Atlanta, Georgia 30332

T. Koutchma

National Center for Food Safety and Technology, Illinois Institute of Technology, Summit-Agro, Illinois 60501

A. T. Giorges and J. A. Pierson

Food Processing Division, Georgia Tech Research Institute, Atlanta, Georgia 30332

To optimize UV disinfection of microbes between concentric cylinders, inactivation in the plug flow reactor geometries of laminar Poiseuille flow, turbulent flow, and laminar Taylor−Couette flow is investigated experimentally and numerically. It is found that there is an optimum ratio of radiation penetration depth to gap width λ/d for each of the three flow patterns. The optimum λ/d for laminar Poiseuille flow, turbulent flow, and laminar Taylor−Couette flow are 1.5, 1, and 0.5, respectively. It is also concluded that laminar Poiseuille flow provides inferior (small) inactivation levels while laminar Taylor−Couette flow provides superior (large) inactivation levels. The relative inactivation levels are as follows: laminar Poiseuille flow < turbulent flow < laminar Taylor−Couette flow.

Introduction

Outbreaks of food-borne illness associated with the consumption of unpasteurized juice and apple cider have resulted in a rule published by the U.S. Food and Drug Administration (FDA) in order to improve the safety of juice products. The rule (21 CFR120) requires manufacturers of juice products to develop a Hazard Analysis and Critical Control Point (HACCP) plan and to achieve a 5-log reduction in the number of the most resistant pathogens.[1] Ultraviolet (UV) disinfection is a promising technology capable of reaching a 5-log reduction of pathogens.

The absorption coefficients of juices typically vary from 10 to 40 cm^{-1} and can be even higher depending on brands and processing conditions. Thin-film annular reactors consisting of two concentric cylinders are suitable for inactivating pathogens in juices. When the two concentric cylinders are fixed, the flow pattern in the gap can be laminar Poiseuille flow or turbulent flow depending on axial hydraulic Reynolds numbers. If the inner cylinder is rotating, and the rotating speed of the inner cylinder exceeds a certain value, the flow pattern can be either laminar or turbulent Taylor−Couette flow depending on the magnitude of the Taylor number.[2,3]

UV disinfection of juice or apple cider in laminar Poiseuille flow and turbulent flow was previously investigated by Wright et al.,[4] Hanes et al.,[5] Koutchma et al.,[6] and Unluturk et al.[7] Recently, Forney et al.[8−10] investigated the possibility of applying laminar Taylor−Couette flow to the UV disinfection of juice. Their preliminary research showed that laminar Taylor−Couette flow largely eliminates the broad fluence distribution resulting from juices with high absorption coefficients compared with laminar Poiseuille flow. In the present study, the three flow patterns have been compared. The optimum gap width for each flow pattern is suggested. The objectives of this study are to (1) compare UV disinfection within reactors experimentally and numerically with three different flow patterns and (2) optimize operating parameters for each flow pattern.

* To whom correspondence should be addressed. Tel: 404-894-2825. Fax: 404-385-2713. E-mail: larry.forney@chbe.gatech.edu.

Experimental Apparatus and Procedure

UV Treatment System in Laminar Poiseuille or Turbulent Flow. The UV treatment system for the study of the effects of laminar Poiseuille or turbulent flow are thin-film annular reactors from UltraDynamics model TF-1535 (Severn Trent Services Inc., Colmar, PA). The whole system consists of four annular reactors with UV lamp lengths of 11.2, 29.2, 77.9, and 77.9 cm. The incident fluence rates on the quartz surface are 15.4, 16, and 12 mW/cm^2, respectively, for the three UV lamps. Each thin-film annular reactor includes a UV lamp at the center of the cylindrical reactor, protective quartz sleeve, fluid within the cylindrical annulus, and a stainless steel outer cylinder. The experiment also included a remote power supply for (120 Vac) (220 Vac) 50/60 operation with a built-in lamp failure indicator. A single low-pressure, germicidal UV lamp was positioned in the center of each 316L stainless steel reactor vessel. The outer radius of the quartz sleeve is $R_1 = 1.225$ cm, and the inner radius of the stainless steel container is $R_2 = 1.79$ cm. Therefore, the fluid gap formed by the two cylinders is $d = R_2 - R_1 = 0.515$ cm. All four reactors are used separately for laminar Poiseuille flow or connected in series for turbulent flow in order to achieve longer residence times as shown in Figure 1.

UV Treatment System in Laminar Taylor−Couette Flow. The schematic diagram of the Taylor−Couette reactor is shown as Figure 2. The stator of the Taylor−Couette UV reactor was constructed of $\Phi_2 = 4.577$ cm internal diameter, fused quartz (Vycor, Corning Inc., Corning, NY) with an internal Teflon rotor of $\Phi_1 = 3.434$ cm outer diameter. The dimensions provided a fluid gap width of $d = 0.5715$ cm. The radiation source consisted of six medium-pressure, mercury UVC lamps with diameters of 0.95 cm and effective lengths of $L = 5.34$ cm (Pen-Ray Lamps, UVP, Upland, CA), which are evenly

10.1021/ie0703641 CCC: $40.75
Published on Web 10/23/2007

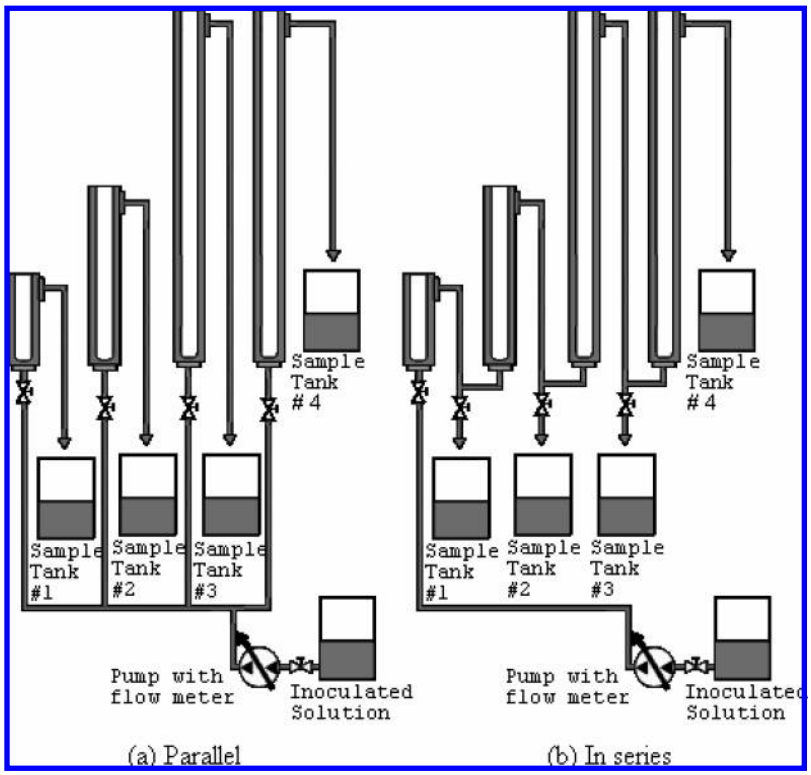

Figure 1. Schematic diagram of the UV treatment system in laminar Poiseuille flow and turbulent flow.

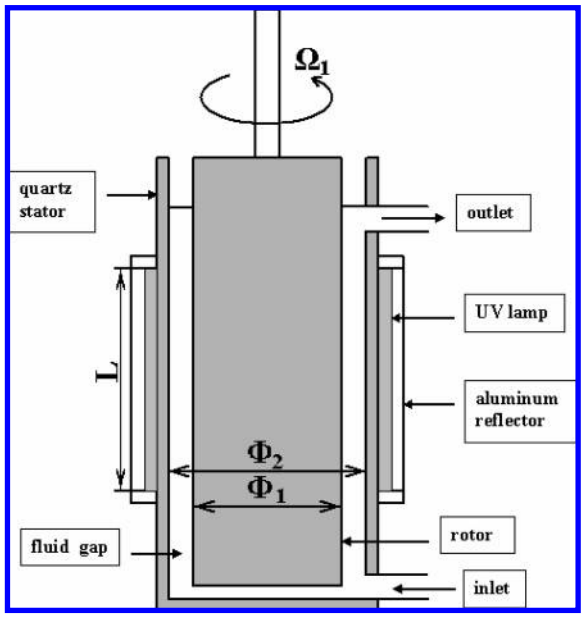

Figure 2. Schematic diagram of the Taylor−Couette UV reactor.

distributed around the outside of the quartz stator. Moreover, the UV lamps are surrounded with an aluminum reflector as shown in Figure 2. The incident radiation fluence rate from the quartz surface into the fluid is assumed to be uniform where $I_o = 25$ mW/cm^2. The Taylor number used to characterize the flow is defined as,

$$Ta = \frac{R_1 \Omega_1 d}{\nu}\left(\frac{\mathrm{d}}{R_1}\right)^{1/2} \quad (1)$$

where R_1 is the radius of the inner cylinder, Ω_1 is the angular velocity of the inner cylinder, d is the gap width, and ν is the kinematic viscosity.

Experimental Procedures. The solution used in the UV disinfection experiments in turbulent flow was commercial clarified apple juice (Ocean Spray, Lakeville-Middleboro, MA). The solutions used in the UV disinfection experiments in both laminar Poiseuille flow and laminar Taylor−Couette flow are model solutions[6] For the latter, Caramel 050 (D.D. Williamson & Co., Inc., Louisville, KY) is added to adjust the absorption coefficient of the fluid.

The solutions inoculated with *Eacherichia coli* K12 (ATCC 25253) or *Yersinia pseudotuberculosis* are pumped into the reactor and irradiated in the gap. Each reactor is mounted in the vertical position with the fluid flowing from the bottom in order to fill the annular gap and avoid bubbles. Samples for microbial analysis are taken after steady-state conditions are reached. The concentrations of viable microorganisms both before and after UV exposure are determined by a place plate method.

UV Inactivation Kinetics

The first-order inactivation model is the simplest used to describe UV inactivation kinetics. The model assumes that the inactivation rate changes with respect to pathogen concentration and fluence rate such that

$$\frac{\mathrm{d}N}{\mathrm{d}t} = -k_1 I N \quad (2)$$

where k_1 is first-order inactivation constant (cm^2/mJ). If k_1 and I are constant, by integration,

$$\frac{N}{N_0} = \exp(-k_1 I t) \quad (3)$$

Because a lag in microbial inactivation at low fluence (the shouldered survival curve) is often observed, the first-order model can overestimate inactivation at low log reduction where

$N \sim N_o$. Therefore, the series-event inactivation model presented by Severin et al.[11] was proposed to account for the lag at low fluence. The model assumes that the inactivation of microorganism elements takes place in a stepwise fashion and the rate at each step is first order with respect to the fluence rate I,

$$\frac{dN_i}{dt} = k_{SE} I (N_{i-1} - N_i) \tag{4}$$

where k_{SE} is the inactivation rate constant in the series-event inactivation model and the subscript i is the event level. Here, k_{SE} is assumed to be the same for different event levels. When n elements of the microorganism (a threshold) have been inactivated, the microorganisms will become nonviable. If k_{SE} and I are constant, the concentration of surviving microorganisms N is determined by

$$\frac{N}{N_0} = \exp(-k_{SE} It) \sum_{i=0}^{n-1} \frac{(k_{SE} It)^i}{i!} \tag{5}$$

where n is a threshold. It is clear that if $n = 1$, the above equation reduces to the first-order model.

Recently, Ye et al.[12] recorded that the inactivation parameters of *E. coli* K12 are $k_1 = 0.325$ cm^2/mJ and $k_{SE} = 0.675$ cm^2/mJ with a threshold $n = 4$ and the inactivation parameters of *Y. pseudotuberculosis* are $k_1 = 0.557$ cm^2/mJ and $k_{SE} = 0.984$ cm^2/mJ with a threshold $n = 3$.

Numerical Simulation

UV Disinfection in Laminar Poiseuille Flow. The UV fluence rate in the annular gap can be approximated by Lambert−Beer's law. If the radiation comes from the inner cylinder, the fluence rate at the radius r becomes

$$I(\mathrm{r}) = I_o \frac{R_1}{\mathrm{r}} \exp(-\alpha(r - R_1)) \tag{6a}$$

where α is the absorbance coefficient (e base) (cm^{-1}), I_o is incident fluence rate, and R_1 is the radius of the inner cylinder. If the radiation comes from the outer cylinder,

$$I(r) = I_o \frac{R_2}{r} \exp(-\alpha(R_2 - r)) \tag{6b}$$

where R_2 is the radius of the outer cylinder.

The governing equations of fluid flow and microorganism concentration can be simplified depending on the flow patterns. For laminar Poiseuille flow,[13] it can be assumed that only an axial velocity component u_z exists and changes with azimuthal angle $\partial/\partial\theta = 0$. Then

$$u_z(r) = C_1 \left[1 - \frac{r^2}{R_2^2} + \frac{1 - \kappa^2}{\ln(1/\kappa)} \ln\left(\frac{r}{R_2}\right)\right] v \tag{7}$$

The average concentration of viable microorganisms at the outlet of the reactor N can now be obtained by numerical integration. For example, if the series-event inactivation model is used,

$$\frac{N}{N_0} = \frac{\int_{R_1}^{R_2} \exp(-k_{SE} I(r) L/u_z(r)) \sum_{i=0}^{n-1} (-k_{SE} I(r) L/u_z(r))^i}{i!\, u_z(r) r\, dr} \int_{R_1}^{R_2} u_z(r) r\, dr \tag{8}$$

UV Disinfection in Turbulent Flow. For turbulent flow, the $k - \epsilon$ model is used to simulate turbulence, and it can also be assumed that only radial and axial velocity components exist and $\partial/\partial\theta = 0$. Then, the governing equations of fluid flow and microorganism concentrations in cylindrical coordinate can be written as[14]

$$\frac{1}{r}\frac{\partial(r u_r)}{\partial r} + \frac{\partial u_z}{\partial z} = 0 \tag{9}$$

$$\frac{1}{\mathrm{r}}\frac{\partial(r\rho u_r \phi)}{\partial r} + \frac{\partial(\rho u_z \phi)}{\partial z} = \frac{1}{r}\frac{\partial}{\partial r}\left(r(\mu + \mu_t)\frac{\partial \phi}{\partial r}\right) + \frac{\partial}{\partial z}\left((\mu + \mu_t)\frac{\partial \phi}{\partial z}\right) + S_\phi \tag{10}$$

$$u_r \frac{\partial N_i}{\partial r} + u_z \frac{\partial N_i}{\partial z} = \frac{\mu_t}{\rho Sc_t}\left(\frac{1}{r}\frac{\partial}{\partial r}\left(r\frac{\partial N_i}{\partial r}\right) + \frac{\partial^2 N_i}{\partial z^2}\right) + k_{SE} I (N_{i-1} - N_i) \tag{11}$$

Here, ρ is density, μ_t is turbulent viscosity, and ϕ in eq 10 can be either u_r, u_z, k, or ϵ. The source term S_ϕ in eq 10 is different depending on the definition of ϕ. Sc_t is the turbulent Schmidt number relating the ratio of the turbulent momentum transport to the turbulent mass transport where the recommended value of Sc_t is 0.8.[14]

UV Disinfection in Laminar Taylor−Couette Flow. For laminar Taylor−Couette flow, the governing equations of fluid flow and microorganism concentrations in cylindrical coordinate can be written as[13]

$$\frac{1}{r}\frac{\partial(r u_r)}{\partial r} + \frac{1}{r}\frac{\partial u_\theta}{\partial \theta} + \frac{\partial u_z}{\partial z} = 0 \tag{12}$$

$$\frac{\partial \phi}{\partial t} + \frac{1}{\mathrm{r}}\frac{\partial(r u_r \phi)}{\partial r} + \frac{1}{r}\frac{\partial(u_\theta \phi)}{\partial \theta} + \frac{\partial(u_z \phi)}{\partial z} = \frac{1}{r}\frac{\partial}{\partial r}\left(r\nu\frac{\partial \phi}{\partial r}\right) + \frac{1}{r}\frac{\partial}{\partial \theta}\left(\frac{\nu}{r}\frac{\partial \phi}{\partial \theta}\right) + \nu\frac{\partial^2 \phi}{\partial z^2} + S_\phi \tag{13}$$

$$\frac{\partial N_i}{\partial t} + u_r\frac{\partial N_i}{\partial r} + \frac{u_\theta}{r}\frac{\partial N_i}{\partial \theta} + u_z\frac{\partial N_i}{\partial z} = D\left(\frac{1}{r}\frac{\partial}{\partial r}\left(r\frac{\partial N_i}{\partial r}\right) + \frac{1}{r^2}\frac{\partial^2 N_i}{\partial \theta^2} + \frac{\partial^2 N_i}{\partial z^2}\right) + k_{SE} I (N_{i-1} - N_i) \tag{14}$$

where ϕ in eq 13 can be either u_r, u_θ, or u_z. The source term S_ϕ is again different depending on the definition of ϕ. Since the molecular diffusion coefficient D is small in eq 14, these diffusion terms can normally be neglected.

Results and Discussion

Comparison between Experimental Results and Numerical Simulation. Figure 3 is the comparison of *E. coli* inactivation between experimental results and numerical simulations for the 77.9-cm reactor in laminar Poiseuille flow. Figure 3 illustrates that numerical simulations agree well with experimental results.

Figure 4 is the comparison of *Y. pseudotuberculosis* inactivation between experimental results and numerical simulations in turbulent flow (axial hydraulic $Re_h\, 2\rho v d/\mu = 2000$) with four reactors connected in series. The juice absorption coefficient is $A = 7.155$ cm^{-1}, and the flow rate is $Q = 120$ mL/s. The small deviation between experimental results and numerical simulations in Figure 4 was probably caused by the assumption that

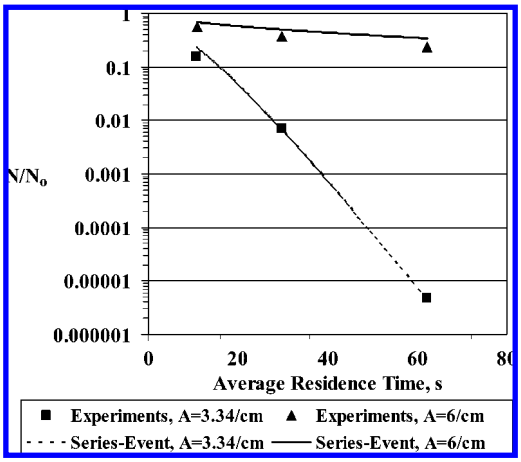

Figure 3. Comparison of *E. coli* inactivation between experimental results and numerical simulations with laminar Poiseuille flow. Reactor length L = 77.9 cm and gap width d = 0.515 cm.

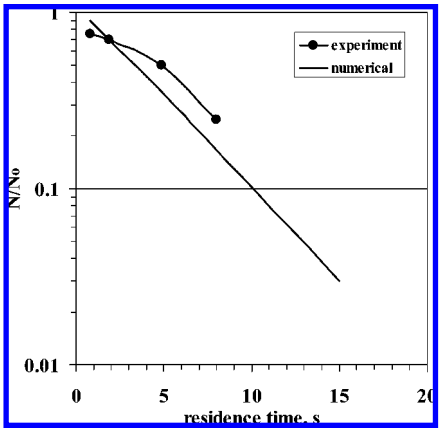

Figure 4. Comparison of *Y. pseudotuberculosis* inactivation between experimental results and numerical simulations in turbulent flow. Gap width d = 0.515 cm.

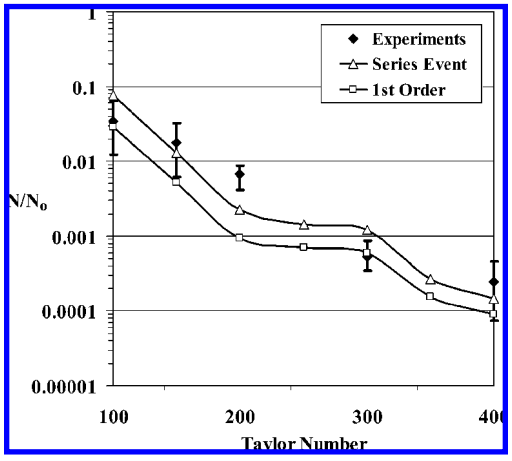

Figure 5. Comparison of *E. coli* inactivation between experimental results and 2D numerical simulations with different Taylor numbers when Q = 40 mL/min, A = 11 cm^{-1}, and d = 0.572 cm.

perfect mixing occurs in the connection tubing between two reactors in series.

Figures 5−7 are the comparison of *E. coli* inactivation between experimental results and numerical simulations in laminar Taylor−Couette flow with different Taylor numbers, average residence times, and penetration depths, respectively. The penetration depth λ is defined as the path length at which the fluence rate is 10% of the incident radiation fluence rate,

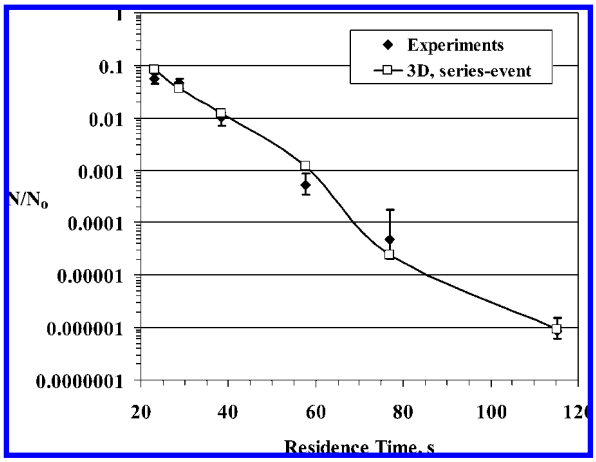

Figure 6. Comparison of *E. coli* inactivation between experimental results and numerical simulations versus average residence time when Ta = 300, A = 11 cm^{-1}, and d = 0.572 cm.

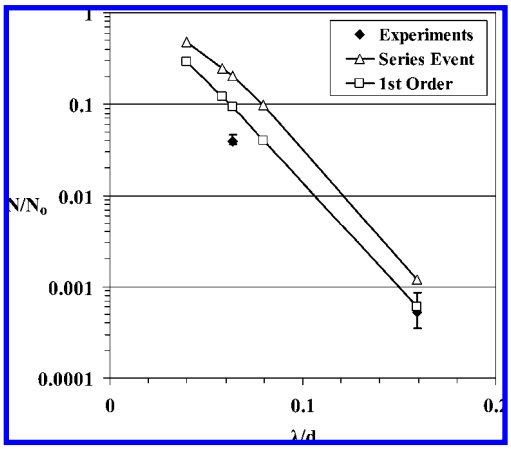

Figure 7. Comparison of *E. coli* inactivation between experimental results and 2D numerical simulations with different penetration depths when Q = 40 mL/min., Ta = 300, and d = 0.572 cm.

namely, $\lambda = -\log(10^{-1})/A$ or $\lambda = 1/A$. The results of Figures 5−7 show that the numerical simulations agree well with experimental results with different operating conditions.

These results suggest that the numerical simulations can predict experimental disinfection in laminar Poiseuille, turbulent and laminar Taylor−Couette flows. Thus, numerical methods will be used to calculate the optimum gap width and compare disinfection among the three flow patterns.

Correlation of UV Disinfection in Turbulent and Taylor−Couette Reactors. If turbulent and Taylor−Couette reactors can be approximated as ideal plug flow reactors (PFRs) and the first-order inactivation model is used, the microbe inactivation is

$$\ln\left(\frac{N}{N_0}\right) = -k_1 I_{av}\tau \tag{15}$$

Here, the average fluence rate is determined by integrating eq 6 or

$$I_{av} = \frac{2\pi\int_{R_1}^{R_2} I_o \frac{R_1}{r}\exp(-\alpha(r-R_1))r\,dr}{2\pi\int_{R_1}^{R_2} r\,dr} = \frac{I_o R_1[1-\exp(-\alpha(R_2-R_1))]}{0.5\alpha(R_2^2-R_1^2)} \tag{16}$$

In eqs 15 and 16, $\tau = L/v$ and the radiation is assumed to irradiate from the inner cylinder. Substitution of eq 16 into eq 15 gives

$$\ln\left(\frac{N}{N_o}\right) = -k_1\frac{R_1[1-\exp(-\alpha(R_2-R_1))]}{0.5\alpha(R_2^2-R_1^2)}I_o\tau \quad (17)$$

For normal values of $\alpha(R_2 - R_1) > 5$ and $\exp(-\alpha(R_2 - R_1)) \ll 1$, eq 17 can be simplified further such that

$$\ln\left(\frac{N}{N_o}\right) = -\frac{k_1 I_o \tau R_c}{\alpha d} \quad (18)$$

where the gap width $d = R_2 - R_1$ and a new dimensionless group is defined as

$$R_c = \frac{2R_1}{R_2 + R_1} \quad (19a)$$

Equation 19a is introduced if the radiation comes from the inner cylinder. If the radiation comes from the outer cylinder,

$$R_c = \frac{2R_2}{R_2 + R_1} \quad (19a)$$

To correct for the effects of the fluid boundary near the radiation surface, it is convenient to add the ratio c/δ to eq 18, where δ is the boundary layer thickness. Thus, eq 18 is modified as

$$\ln\left(\frac{N}{N_o}\right) = -\frac{ckI_o\tau R_c}{\alpha d\delta} \quad (20)$$

The boundary layer thickness δ for turbulent flow in eq 20 is calculated according to eq 21 from Middleman[15]

$$\delta = \frac{2\mu}{\rho v f} \quad (21)$$

where f is the dimensionless shear stress or friction factor. According to boundary layer theory,[16] the friction factor f can be approximated by

$$f = 0.079Re_h^{-0.25} \quad (22)$$

where $Re_h = 2\rho dv/\mu$ is the hydraulic Reynolds number for flow between concentric cylinders. In contrast, for laminar Taylor−Couette flow, the boundary thickness δ is proportional to $Ta^{-1/2}$ from the work of Baier et al.[17] and Forney et al.[8,9] where

$$\delta = 2d/\sqrt{Ta} \quad (23)$$

The experimental data of both turbulent and laminar Taylor−Couette reactors are correlated with the same dimensionless group as shown in Figure 8. Here, the constant $c = 0.0125$ cm in eq 20 for the solid line is obtained by the least-squares method. The standard deviation between the data and eq 20 is minimized such that $\sigma_y = 0.283$ and the coefficient of determination $R^2 = 0.973$ in Figure 8. Figure 8 shows that the same correlation equation can be used to predict UV disinfection for both turbulent and laminar Taylor−Couette reactors. Similarly, the numerical results of both turbulent reactors and laminar Taylor−Couette reactors are correlated with eq 20 and are shown in Figure 9.

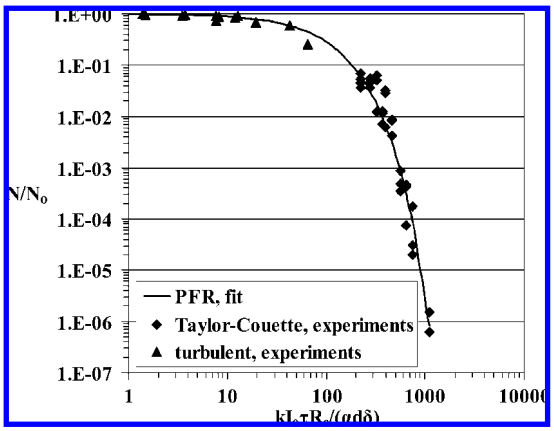

Figure 8. Correlation of experimental data for UV disinfection in turbulent and laminar Taylor−Couette reactors.

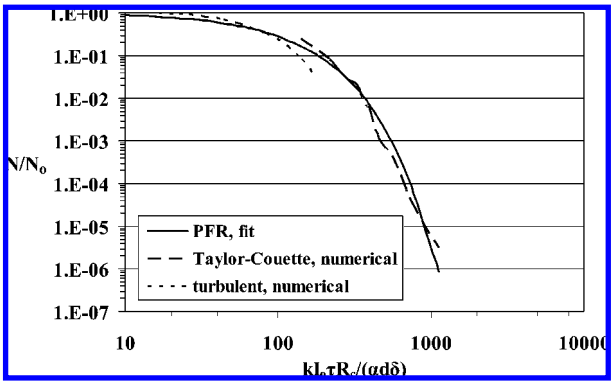

Figure 9. Correlation of numerical results for UV disinfection in turbulent and laminar Taylor−Couette reactors.

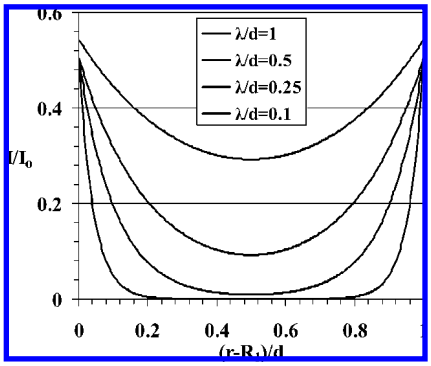

Figure 10. Profile of radiation intensity across the gap for laminar, turbulent or Taylor- Couette flow. Order of λ/d values in caption is the same order in graph.

Optimum Gap Width. Gap width is one of the most important parameters for the design of thin-film annular UV reactors. For simplicity, one considers radiation from both the inner and outer walls of a concentric cylinder geometry as shown in Figure 10. Tracing a path across the fluid gap provides profiles of possible radiation intensity that are shown in Figure 10. For example, microbes at the center of the gap are subjected to a small radiation intensity that is shown on a single curve at the center of Figure 10. Moreover, microbes near the wall experience a larger radiation intensity. Consider constant flow rate in Figure 10, where the fluid velocity v is inversely proportional to the gap width or $v\alpha 1/d$. Thus, contours at the top of Figure 10, where the gap width d is small, subject microbes to a large radiation intensity but short residence times. Conversely, if d is large, microbes across the gap are subject to a small radiation intensity representative of the bottom contour

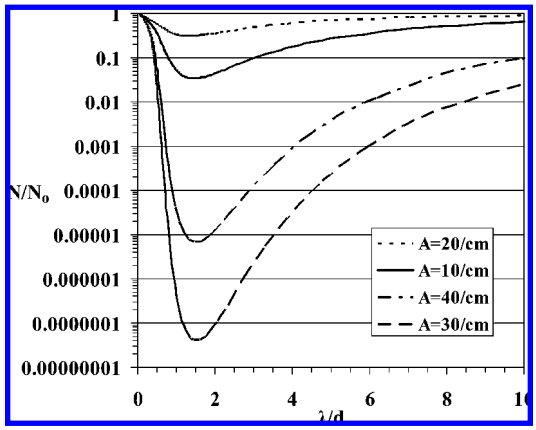

Figure 11. Optimum λ/d in laminar Poiseuille flow.

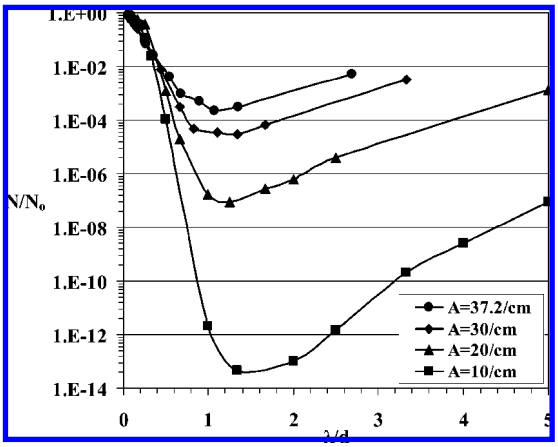

Figure 12. Optimum λ/d in turbulent flow.

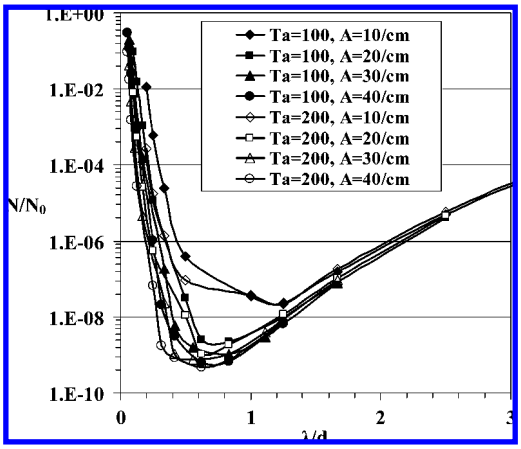

Figure 13. Optimum λ/d in laminar Taylor−Couette flow.

in Figure 10 but large residence times. Thus, the average dosage of photons $I_{av}\tau$ is low on both the top and bottom contours of Figure 10 but high for intermediate contours for both laminar, turbulent and Taylor−Couette flows.

Figures 11−13 show how microbe inactivation levels change with λ/d when the radius of inner cylinder is constant at 1.225 cm and radiation comes from the inner cylinder. The radius of the outer cylinder is changed to create different gap widths. According to Figures 11−13, there is an optimum gap width for each absorption coefficient. Although the optimum λ/d is somewhat different because of different conditions such as absorption coefficients and flow patterns, the optimum λ/d oscillates around a fixed value for each flow pattern. The optimum λ/d for laminar Poiseuille flow, turbulent flow, and laminar Taylor−Couette flow are 1.5, 1, and 0.5, respectively.

For laminar Poiseuille flow, the optimum $\lambda/d = 1.5$ in Figure 11. When $\lambda/d < 1.5$, a longer residence time results in pathogens that are partially overexposed to the radiation source. However, disinfection of the overexposed fraction near the radiation source cannot offset the increase in surviving pathogens of the under exposed fraction across the wider gap width. According to Figure 11, inactivation levels decrease greatly when $\lambda/d < 1.0$. For example, when $\lambda/d = 0.2$, the inactivation level is about 5% of the optimum. Finally, since $\lambda = 1/A$, Figure 11 can be used to design a laminar UV reactor to achieve a 5-log reduction where $\lambda/d \sim 1.0$.

There is an optimum gap width for each absorption coefficient in turbulent flow as was the case for laminar flow. Figure 12 shows how *Y. pseudotuberculosis* microbe reductions change with gap width when the radius of the inner cylinder is constant at 1.225 cm while the radius of the outer cylinder is changed. In Figure 12, the series event model is used with $k_{SE} = 0.984$ cm^2/mJ and $n = 3$ and radiation comes from the inner cylinder with a fluence rate of $I_o = 800$ mW/cm^2 for a UV lamp length of $L = 29.2$ cm.

From Figure 12, it is shown that the optimum $\lambda/d \sim 1.0$ for turbulent flow and does not change dramatically for different absorption coefficients. As shown, the penetration depth equals the gap width for optimum disinfection in turbulent flow or the radiation has to penetrate across the gap to obtain optimum disinfection. This requirement is caused by the underirradiated region in the viscous sublayer[18] on the opposite side of the radiation source. Though the underirradiated region occupies only a small fraction of the gap, ~5% or less, surviving pathogens in the underirradiated region contribute to the population of surviving pathogens within the gap. Because most of pathogens in the underirradiated region survive if $\lambda/d \ll 1$, the average concentration of the surviving pathogen at the outlet will be $\sim 0.05N_o$. Since the normal absorption coefficients of juices are 10−40 cm^{-1}, the optimum gap width is in the range of 0.25−1.0 mm. Therefore, the gap width of turbulent UV reactors used for juice disinfection should not be more than 1.5 mm.

One method to improve the performance of the turbulent UV reactor and to eliminate the viscous sublayer problem is to irradiate from both of the cylinders. Another method is to connect the UV reactors in series. In the latter case, pathogens in the viscous sublayer in the first UV reactor may enter the fully turbulent region in the next reactor. Moreover, the short residence time for turbulent flow conditions may also require that one connect several reactors in series.

Figure 13 illustrates that optimum inactivation occurs at a ratio of $\lambda/d = 0.5$ for all fluids in Taylor−Couette flow. As is the case with both laminar and turbulent flows, the inactivation level of microbes in Taylor−Couette flow is affected by the absorbance $A = 1/\lambda$, in particular, the ratio of penetration depth to gap width λ/d. For example, if one wishes to achieve a 5-log reduction ($N/N_o = 10^{-5}$) in viable microbes with the Taylor−Couette device, the design would require a somewhat larger gap width with $\lambda/d < 0.5$. Because the normal absorption coefficients of juices are 10−40 cm^{-1}, the optimum gap width is in the range of 0.5−2.0 mm. Therefore, the gap width of Taylor−Couette UV reactors used for juice disinfection should not be more than 3 mm.

Optimum Inactivation among Three Flow Patterns. Because of different requirements for the three flow patterns, it is impossible to compare microbe inactivation at the same condi-

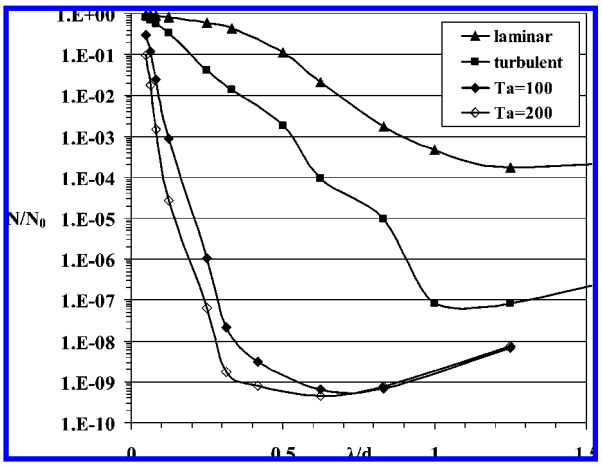

Figure 14. Comparison of inactivation for three flow patterns. Dosage is $I_o\tau = 2870$ mJ/cm^2 and absorption coefficient $A = 40$ cm^{-1}.

tions such as flow rate. However, theoretical predictions suggest similar inactivation levels for the same radii of the cylinders, pathogen and fluence $I_o\tau$. Figure 14 is the comparison of log reductions among the three flow patterns, where the radius of the inner cylinder is 1.225 cm and series-event inactivation model of *E. coli* is used. In Figure 14, the radius of the outer cylinder is changed from 1.235 to 1.74 cm in order to create different gap widths.

According to Figure 14, laminar Taylor−Couette flow is superior to either turbulent or laminar Poiseuille flow in the following aspects:

(1) Laminar Taylor−Couette flow achieves inactivation levels superior to either laminar Poiseuille or turbulent flow with the same dosage $I_o\tau$, absorption coefficient A, and flow rates. For example, when $A = 40$ cm^{-1} and $\lambda/d = 0.417$, the inactivation levels $N/N_0 = 8.2 \times 10^{-10}$, 8.1×10^{-3}, and 0.27 for laminar Taylor−Couette flow ($Ta = 200$) and turbulent and laminar Poiseuille flow, respectively. Both turbulent and laminar Poiseuille flows achieve small inactivation levels when the absorption coefficients of juices are high and λ/d is small. For example, when $A = 40$ cm^{-1} and $\lambda/d = 0.049$, the inactivation levels N/N_0 are 0.81 and 0.95 for turbulent flow and laminar Poiseuille flow, respectively. However, $N/N_0 = 0.097$ for laminar Taylor−Couette flow ($Ta = 200$).

(2) As stated earlier, the optimum λ/d for laminar Taylor−Couette flow is reduced to 0.5 compared with the optimum λ/d of 1.5 and 1.0 for laminar Poiseuille and turbulent flow, respectively. Thus, laminar Taylor−Couette flow is suitable for disinfecting juices with large absorption coefficients.

Fluence Distribution Function among Three Flow Patterns. One objective with the design of UV reactors is to provide an equal flux of photons to each microbe. Providing a uniform photon flux to each microbe is difficult because of the attenuation of the photon flux with distance from the radation source near the wall. The only way to overcome a nonuniform photon flux is to provide sufficient microbe transport or mixing within the fluid gap. Figure 15 illustrates fluid streamlines containing microbes that result from Taylor−Couette flow. Included in Figure 15 are streamlines with a conventional design and a design with a wavy wall configuration.

One method of comparing the effects of different flow patterns within a plug flow reactor is to determine the fluence distribution. The fluence distribution is computed by following a large number of microbes through the reactor while summing the number of photons incident on each microbe.

Figure 16 is the fluence distribution function of the three flow

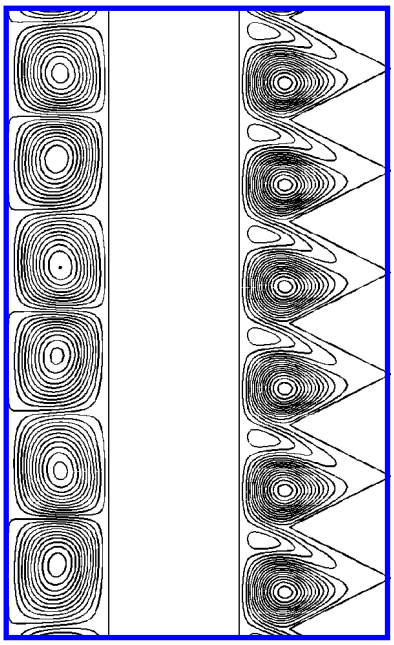

Figure 15. Fluid streamlines in Taylor−Couette flow. Flat rotor in left figure, $d = 2$ mm. Wavy rotor in right figure, wavelength $Lw = 2$ mm, wave amplitude $h = 1$ mm, and $d = 2$ mm.

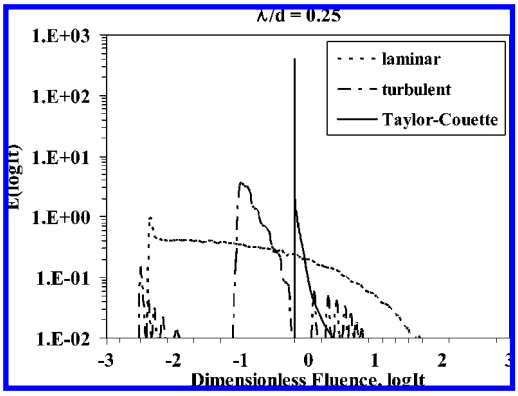

Figure 16. Fluence distribution for three flow patterns. $Ta = 200$ for Taylor−Couette flow, $A = 10$ cm^{-1}, and $d = 4$ mm.

patterns when $\lambda/d = 0.25$. The fluence distribution function is defined as the fraction of fluids leaving the reactor that has fluence of (logIt, logIt + d(logIt))

$$E(\log It)\,\mathrm{d}(\log It) = \text{fraction of fluids with fluence of } (\log It, \log It + \mathrm{d}(\log It)) \quad (24)$$

where the fluence It is made dimensionless by the average fluence of an ideal plug flow reactor (see eq 16). The fluence distribution function E(logIt) is defined by the expression given by Forney et al.[10]

$$E(\log It) = \frac{1}{N_T}\frac{\mathrm{d}N}{\mathrm{d}(\log It)} \quad (25)$$

In Figure 16, the area under the curve for each reactor design represents all microbes tracked for each design or $\int E(\log It)\,\mathrm{d}(\log It) = 1$. In simple terms, reactor designs with the highest peaks in the distribution function are superior. In such designs, all microbes are subject to a nearly uniform number of photons and the required incident radiation flux for inactivation is reduced.

According to Figure 16, Taylor vortex reactors approach the superior characteristics of a PFR. Moreover, for turbulent flow,

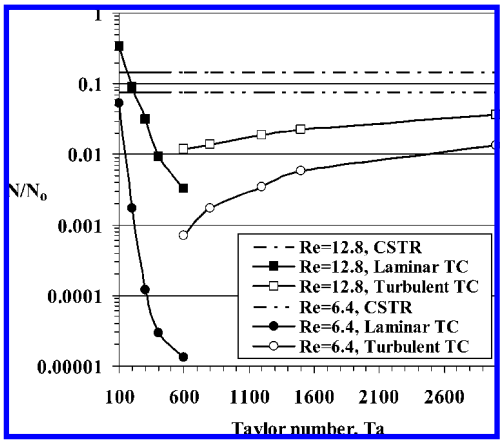

Figure 17. Microbe inactivation for laminar and turbulent Taylor−Couette flow. Axial $Re = Re_h$ the hydraulic Reynolds number

there are three peaks. The left peak corresponds to the effect of the viscous sublayer on the opposite side of the radiation source while the right peak corresponds to the effect of the viscous sublayer near the radiation source. Finally, the middle peak corresponds to the effect of the fully turbulent region.

Conclusions

UV disinfection between concentric cylinders in laminar Poiseuille flow, turbulent flow, and laminar Taylor−Couette flow was investigated experimentally and numerically. Numerical simulations agree well with experimental results. Laminar Taylor−Couette flow is superior to either turbulent or laminar Poiseuille flow for the following reasons:[19] (1) laminar Taylor−Couette flow always achieves larger log reduction levels than either laminar Poiseuille or turbulent flow with the same dosage $I_o\tau$, pathogen and cylinder radii. (2) the optimum λ/d for laminar Taylor−Couette flow is reduced to 0.5 compared with the optimum λ/d of 1.5 and 1.0 for laminar Poiseuille flow and turbulent flow, respectively.

Therefore, laminar Taylor−Couette reactors are suitable for processing a variety of juices, especially those with large absorption coefficients. In contrast, for laminar Poiseuille flow, the optimum gap width is very small in the absence of radial mixing. Inactivation decreases sharply if the gap width of the reactor is larger than the optimum. The laminar Poiseuille reactors are suitable for water or wastewater, for which the absorption coefficient is small. Improvements in the performance of laminar UV reactors are achieved in practice by redistributing the fluid at two or more locations along the reactor axis.[6]For turbulent flow, the high flow rate to ensure turbulence is coupled with a reduced residence time. The turbulent reactors are suitable for processing large quantities of juice, for which penetration depth is much larger than the viscous sublayer thickness.

Acknowledgment

FoodPAC (Food Processing Advisory Council for the State of Georgia) is gratefully acknowledged for financial support.

Appendix A

Turbulent Taylor−Couette Flow. Experiments by Lueptow et al.[3] show that the flow pattern in the annular gap will change from laminar Taylor−Couette to turbulent Taylor−Couette flow with an increase in Taylor number. Figure 17 shows the log reductions of *E. coli* including laminar and turbulent Taylor−Couette flow. In Figure 17, the axial Reynolds numbers are 6.4 and 12.8 for flow rates 0.3 and 0.6 mL/s, respectively. The radii of the inner and outer cylinder are 1.225 and 1.74 cm, respectively. The length of the UV lamp is 11.2 cm, and UV is irradiated from the inner cylinder with an intensity of 12 mW/cm^2. In Figure 17, the series-event inactivation model of *E. coli* is used and the absorption coefficient is assumed to be $A = 20$ cm^{-1}. Since it is difficult to determine the exact Taylor number at which the transition from laminar to turbulent flow occurs,[3] both laminar and turbulent simulation results with $Ta = 600$ are provided.

In laminar Taylor−Couette flow, the inactivation levels increase with Taylor number as shown in Figure 5. In Figure 17, it is shown that log reductions in turbulent Taylor−Couette flow do not increase with Taylor number. On the contrary, the log reductions in turbulent Taylor−Couette flow will decrease with an increase in Taylor number where the latter is caused by axial turbulent mixing. Turbulent Taylor−Couette flow increases both the radial and axial mixing, where the latter should be avoided in the thin-film annular reactors. The axial mixing at large *Ta* number is a kind of back-mixing and will reduce disinfection results. With the increase in Taylor number in turbulent Taylor−Couette flow, the flow pattern is approaching that of a continuous stirred tank reactor as demonstrated by Resende et al.[20] By contrast, the axial mixing is negligible in laminar Taylor−Couette flow, which can be approximated by an ideal PFR as shown by Kataoka et al.[21] Therefore, the Taylor vortex reactors should be operated in laminar Taylor−Couette flow and with Taylor numbers as high as possible.[22]

Nomenclature

A = absorption coefficient with 10 base, cm^{-1}, $I_x = I_o \times 10^{(-Ax)}$
c = a constant to correct for deviations between reactors, cm
C_1 = constant determined by κ, $C_1 = 2/(1 + \kappa^2 - (1 - \kappa^2)/\ln(1/\kappa))$
d = gap width, cm
f = dimensionless shear stress, Pa
i = event level
I_o = incident fluence rate, mW/cm^2
$I(r)$ = fluence rate at a position in the gap r, mW/cm^2
It = fluence, mJ/cm^2
$I_{av}\tau$ = average fluence of ideal plug flow reactor, mJ/cm^2
k = turbulent kinetic energy, m^2/s^2 or inactivation constant, cm^2/mJ
k_1 = inactivation constant of the first inactivation model, cm^2/mJ
k_{SE} = inactivation constant of the series-event inactivation model, cm^2/mJ
L = length of radiation section, cm
n = threshold for inactivation in the series-event model
N = concentration of viable microorganisms, cfu/mL
N_o = concentration of viable microorganisms before exposure, cfu/mL
N_i = concentration of viable microorganisms at event level i, cfu/mL
Q = volumetric flow rate, mL/s
r = radius, cm
R_1 = radius of inner cylinder, cm
R_2 = radius of outer cylinder, cm
Rc = dimensionless group
Re_h = hydraulic Reynolds number, $2d\rho v/\mu$
S_ϕ = source terms depending on the definition of ϕ
Sc_t = turbulent Schmidt number
t = time, s
Ta = Taylor number

u_r = radial velocity component, cm/s
u_z = axial velocity component, cm/s
u_θ = azimuthal velocity component, cm/s
u_τ = friction velocity, m/s
v = average velocity, cm/s or m/s, $= Q/(\pi(R_2^2 - R_1^2))$
z = axial coordinate, cm
α = absorption coefficient with e base, cm^{-1}, $I_x = I_o \exp(-\alpha x)$
ϵ = dissipation rate, m^2/s^3
δ = boundary layer thickness, cm
θ = angle around the cylinder, degree, $0 \leq \theta \leq 2\pi$
κ = ratio of the radius of the inner cylinder to that of outer cylinder, $\kappa = R_1/R_2$
λ = penetration depth, cm, $\lambda = 1/A$
μ = dynamic viscosity, Pa·s
μ_t = turbulent viscosity, Pa·s
ν = kinematic viscosity, m^2/s
ρ = density, kg/m^3
τ = average residence time, s, $= L/v$
θ = variable in governing equations
Ω_1 = angular velocity of inner cylinder, s^{-1}
Φ_1 = outer diameter of inner cylinder, cm
Φ_2 = inner diameter of outer cylinder, cm

Literature Cited

(1) U.S. FDA, 21 CFR Part, 179. Irradiation in the Production, Processing and Handling of Food. *Fed. Regist.* **2000**, *65*, 71056−71058.

(2) Taylor, G. I. Stability of a Viscous Liquid Contained between Two Rotating Cylinders. *Proc. R. Soc., London, Ser. A* **1923**, *223*, 289−343.

(3) Lueptow, R. M.; Dotter A.; K. Min. Stability of axial flow in an annulus with a rotating inner cylinder. *Phys. Fluids* **1992**, *4*, 2446−2455.

(4) Wright, J. R.; Sumner, S. S.; Hackney, C. R.; Pierson, M. D.; Zoecklein, B. W. Efficacy of Ultraviolet Light for Reducing *Escherichia Coli* O157:H7 in Unpasteurized Apple Cider. *J. Food Prot.* **2000**, *63*, 563−567.

(5) Hanes, D. E.; Orlandi, P. A.; Burr, D. H.; Miliotis, M. D.; Robi, M. G.; Bier, J. W.; Jackson, G. J.; Arrowood, M. J.; Churey, J. J.; Worobo, R. W. Inactivation of *Crytosporidium Parvum Oocysts* in Fresh Apple Cider Using Ultraviolet Irradiation. *Appl. Environ. Microbiol.* **2002**, *68*, 4168−4172.

(6) Koutchma, T.; Keller, S.; Chirtel, S.; Parisi, B. Ultraviolet Disinfection of Juice Products in Laminar and Turbulent Flow Reactors. *Innovative Food Sci, Emerging Technol.* **2004**, *5*, 179−189.

(7) Unluturk, S. K.; Arastoopour, H.; Koutchma. T. Modeling of UV Dose Distribution in a Thin-Film UV Reactors for Processing of Apple Cider. *J. Food Eng.* **2004**, *65*, 125−136.

(8) Forney, L. J.; Goodridge, C. F.; Pierson, J. A. Ultraviolet Disinfection: Similitude in Taylor−Couette and Channel flow. *Environ. Sci. Technol.* **2003**, *37*, 5015−5020.

(9) Forney, L. J.; Pierson, J. A. Optimum photolysis in Taylor−Couette flow. *AIChE J.* **2003**, *49*, 727−733.

(10) Forney, L. J.; Pierson, J. A.; Ye, Z. Juice Irradiation with Taylor−Couette Flow: UV Inactivation of *Escherichia Coli*. *J. Food Prot.* **2004**, *67*, 2410−2415.

(11) Severin, B. F.; Suidan, M. T.; Engelbrecht, R. S. Kinetic Modeling of U. V. Disinfection of Water. *Water Res.* **1983**, *17*, 1669−1678.

(12) Ye, Z.; Koutchma, T.; Parisi, B.; Larkin, J.; Forney, L. J. Ultraviolet Inactivation Kinetics of *E. coli and Y. pseudotuberculosis* in Annular Reactors. *J. Food Sci.* **2007**, *72*, E271–E278.

(13) Bird, R. B.; Stewart, W. E.; Lightfoot., E. N. *Transport Phenomena*, 2nd ed.; Wiley: New York, 2002.

(14) Fox, R. O. *Computational Models for Turbulent Reacting Flows*; Cambridge University Press: New York, 2003.

(15) Middleman, S. *An Introduction to Mass and Heat Transfer: Principles of Analysis and Design*; John Wiley & Sons, Inc.: New York, 1998.

(16) Schlichting, H. and Gersten, K. *Boundary-Layer Theory*; Springer-Verlag: Berlin, 2000.

(17) Baier, G.; Grateful, T. M.; Graham, M. D.; Lightfoot, E. N. Prediction of mass transfer in spatially periodic systems. *Chem. Eng. Sci.* **1999**, *54*, 343−355.

(18) Davidson, P. A. *Turbulence: An Introduction for Scientists and Engineers*; Oxford University Press: New York, 2004.

(19) Forney and Pierson, Systems and Methods for Disinfection, 2006, U.S. Patent 7,001,571.

(20) Resende, M. M.; Vieira, P. G.; Sousa, R.; Giordano, R. L. C.; Giordano, R. C. Estimation of Mass Transfer Parameters in a Taylor−Couette-Poiseuille Heterogeneous Reactor. *Braz. J. Chem. Eng.* **2004**, *21*, 175−184.

(21) Kataoka, K.; Doi, H.; Hongo, T.; Futagawa, M. Ideal plug-flow properties of Taylor vortex flow. *J. Chem. Eng. Jpn.* **1975**, *8*, 472−476.

(22) Ye, Z. UV Disinfection Between Concentric Cylinders. Ph.D. Thesis, School of Chemical & Biomolecular Engineering, Georgia Institute of Technology, 2007.

Received for review March 9, 2007
Revised manuscript received August 8, 2007
Accepted August 10, 2007

IE0703641